Available online at www.sciencedirect.com
ScienceDirect
Trans. Nonferrous Met. Soc. China 29(2019) 358−364
Transactions of Nonferrous Metals Society of China
www.tnmsc.cn

Non-isothermal nano-crystallization kinetics in amorphous $Ni_{55}Nb_{35}Si_{10}$ alloy

H. MINOUEI[1], G. H. AKBARI[1], M. H. ENAYATI[2], S. I. HONG[3]

1. Department of Metallurgy and Materials Science, Shahid Bahonar University, Kerman, Iran;
2. Department of Material Engineering, Nanotechnology and Advanced Material Institute, Isfahan University of Technology (IUT), Isfahan, Iran;
3. Department of Nanomaterials Engineering, Chungnam National University, Daejeon 305-764, Korea

Received 8 March 2018; accepted 26 August 2018

Abstract: The non-isothermal crystallization kinetics of $Ni_{55}Nb_{35}Si_{10}$ amorphous alloy, prepared by mechanical alloying, was studied using differential scanning calorimetry. The amorphous alloy showed one-stage crystallization on heating, which led to the formation of nano-intermetallic crystals in amorphous matrix. The apparent activation energy for the crystallization of the alloy, determined by the Kissinger equation, was relatively high (468 kJ/mol), indicating that this amorphous alloy has high thermal stability. Changes in the activation energy during the crystallization process, were also evaluated by iso-conversional methods. The results showed that it decreases slowly from the beginning to crystallized fraction α=0.35 and it remains almost constant to the end of the process. The nano-crystallization mechanism for the non-isothermal crystallization of the amorphous alloy was explained by determining Avrami exponents. Transmission electron microscopy studies revealed the microstructural modification of amorphous alloy via nano-crystallization during annealing. The results suggest that the nucleation rate decreases with increasing time and the crystallization mechanism is governed dominantly by a three-dimensional diffusion-controlled growth. A predictive equation was obtained based on the Sestak−Berggren autocatalytic model to describe quantitatively the non-isothermal crystallization kinetics.
Key words: amorphous alloy; kinetics; nano-crystallization; DSC; activation energy

1 Introduction

Amorphous alloys have been considered attractive for structural applications because of their excellent mechanical properties combined with good corrosion resistance [1−3]. Ni-based amorphous alloys are one of the most important alloys to consider for their relatively high strength and hardness compared to other amorphous materials [4−6]. Among various Ni-based alloys, Ni−Nb system has attracted the interest of many investigators due to its high glass forming ability and good thermal stability [7]. Mechanical alloying method has been considered as a suitable method for the fabrication of several advanced materials [8]. The synthesis of $Ni_{60}Nb_{40}$ amorphous alloy by mechanical alloying technique was reported by KOCH et al [9].

Crystallization kinetics is a topic of considerable interest to study the thermal stability of amorphous structures. The crystallization process of amorphous phase can be utilized as a solid-state processing route for the fabrication of nanostructured materials. The partial or full crystallization of amorphous alloys may lead to the nano-structural modification with various attractive properties [10−12].

Amorphization of Ni−Nb−Si during mechanical alloying operation of elemental powder mixture and the detailed structural evolution has been reported elsewhere [13]. We reported in the previous publication that nano-crystallization of Ni−Nb−Si amorphous alloys leads to the formation of nano-metric phases suppress shear sliding of the amorphous matrix. Therefore, controlled partial crystallization of amorphous alloys in Ni−Nb−Si system is essential in attaining enhanced mechanical properties [13]. The kinetics study can provide important information on nucleation and growth mechanisms associated with crystallization in amorphous alloy, thereby providing a right direction to improve its properties.

Differential scanning calorimetry (DSC) technique is widely used to study crystallization kinetics of amorphous alloys [14]. Generally, crystallization kinetics

Corresponding author: H. MINOUEI; E-mail: h_minouie@yahoo.com
DOI: 10.1016/S1003-6326(19)64945-9

of amorphous alloys is investigated in two basic independent methods: (1) non-isothermal method at a constant linear heating rate and (2) isothermal crystallization kinetics. Non-isothermal experiments are more widely employed due to their easiness and convenience over isothermal experiments in a wide temperature range. The analyses of thermal behavior of the mechanically alloyed amorphous powders and nano-crystallization kinetic parameters, such as the activation energy and the Avrami exponent, n, could render the understanding of the dominant nucleation and growth mechanism in various crystallization stages [15].

The activation energy can also be evaluated by iso-conversional methods [16]. The general form of the linear equation expressing the linear integral iso-conversional methods for calculation of activation energy at a given conversion fraction (E_α) is

$$\ln\left(\frac{\beta_i}{T^B_{\alpha,i}}\right)=\text{Const}-C\frac{E_\alpha}{RT_{\alpha,i}} \quad (1)$$

where β is heating rate, R is the universal gas constant, and B and C are determined by temperature integral approximation. The Kissinger−Akahira−Sunose (KAS), (B=2 and C=1), and Flynn−Wall−Ozawa (FWO), (B=0 and C=1.052), methods have been employed to obtain the function of local activation energy on crystallization fraction [17−20].

The main purpose of this research is studying the kinetics of nano-crystallization process and understanding the crystallization mechanism in Ni−Nb−Si amorphous alloys. The accurate analyses of the activation energies of crystallization as well as other kinetic parameters by analyzing DSC nonisothermal experiments and the comparison with those of various crystallization models are made.

2 Experimental

The amorphous $Ni_{55}Nb_{35}Si_{10}$ (wt.%) alloy was fabricated by mechanical alloying in a planetary ball mill (Fritsch Pulverisette5) under an argon atmosphere for 12 h. High-purity, crystalline Ni, Nb and Si powders were loaded into a hardened chromium steel grinding bowl (120 mL). The mechanical alloying operation was performed at a rotational speed of 300 r/min and a ball-to-powder mass ratio of 10:1.

The microstructures of the amorphous and annealed alloys were investigated by high-resolution transmission electron microscope (HRTEM) (FEI Tecnai G2 F30 S-TWIN) and a selected area diffraction pattern (SADP). Analysis was performed at an acceleration voltage of 300 kV with a resolution of 0.19 nm.

The nano-crystallization kinetics of amorphous alloys was investigated with a DSC instrument (INSEIS L81 II−1550) using a continuous heating method at six different heating rates of 2.5, 5, 10, 20, 30, 40 and 60 °C/min. An argon gas flow was used for the bowl atmosphere. Base line calibration has been performed for each heating rate under identical experimental conditions using the same pair of empty alumina pans on both sides of the DSC cradle.

3 Results and discussion

3.1 Characterization

Figure 1(a) shows the HRTEM image, SADP and Fast Fourier Transform (FFT) of $Ni_{55}Nb_{35}Si_{10}$ powder milled for 12 h. As seen, a fully amorphous structure has been developed by mechanical alloying. Figure 1(b) illustrates the HRTEM image, SADP and FFT of $Ni_{55}Nb_{35}Si_{10}$ powder after annealing for 1 h at 900 °C. Partial crystallization during annealing has led to the formation of nano-crystalline intermetallic particles with average sizes below 10 nm in the amorphous matrix. It

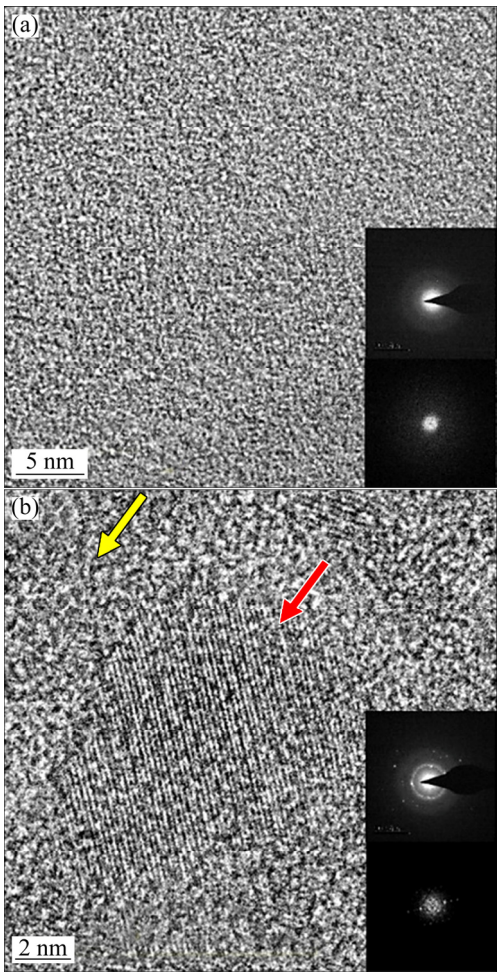

Fig. 1 HRTEM image, SADP and FFT of $Ni_{55}Nb_{35}Si_{10}$ alloy milled for 12 h (a) and after nano-crystallization through annealing at 900 °C for 1 h (b)

was shown that the crystalline phases of Ni_3Nb, Ni_6Nb_7 and Nb_3Ni_2Si have precipitated during crystallization of $Ni_{55}Nb_{35}Si_{10}$ amorphous alloy [13]. Crystalline phases (indicated by a red arrow) surrounded by amorphous phases (indicated by a yellow arrow) are shown in Fig. 1(b). The thermal stability of the remaining amorphous phase is likely to be enhanced owing to the enrichment of the solute elements rejected from the primary crystalline-phase formation. The presence of the stable amorphous phase remaining even after 60 min at 900 °C strongly supports the enhanced stability of remaining amorphous phase after partial crystallization [13].

Figure 2 shows the DSC curves obtained during constant heating for the $Ni_{55}Nb_{35}Si_{10}$ amorphous alloy at different heating rates. It can be seen that T_x (onset crystallization temperature) and T_p (peak temperature), shifted towards higher temperature as the heating rate increased. As seen, the crystallization of $Ni_{55}Nb_{35}Si_{10}$ amorphous alloys occurs in single stage around 680−780 °C. The phase characterization of $Ni_{55}Nb_{35}Si_{10}$ alloy after DSC run was discussed in the previous work [13]. DSC traces also indicated that the remained amorphous phase after crystallization, is stable up to 900 °C. However, crystallization of remained amorphous phase will occur at higher temperature.

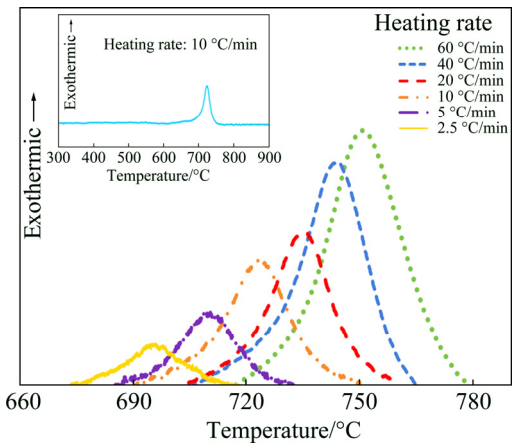

Fig. 2 DSC traces of $Ni_{55}Nb_{35}Si_{10}$ amorphous alloy at various heating rates

The degrees of crystallization α (in volume fraction) as a function of temperature at different heating rates obtained from DSC data are shown in Fig. 3. The fractional conversion curves in Fig. 3 are all sigmoidal in shape, suggesting the presence of incubation periods for all heating rates.

3.2 Non-isothermal crystallization kinetics

3.2.1 Evaluation of activation energy by Kissinger equation

The apparent activation energy for crystallization process was determined by using the well-known Kissinger equation [17]:

$$\ln(\beta/T_p^2)=-E_a/(RT)+\text{const} \quad (2)$$

where T_p represents the peak temperature of crystallization, and E_a is the apparent activation energy of crystallization. Plotting $\ln(\beta/T^2)$ vs $1/T$, gives a straight line, as shown in Fig. 4. The slope of the line yields the value of the crystallization activation energy, E_a=468 kJ/mol. The higher value of activation energy for crystallization in Ni−Nb−Si alloy, compared with other Ni-based amorphous alloys [21], indicates its higher thermal stability.

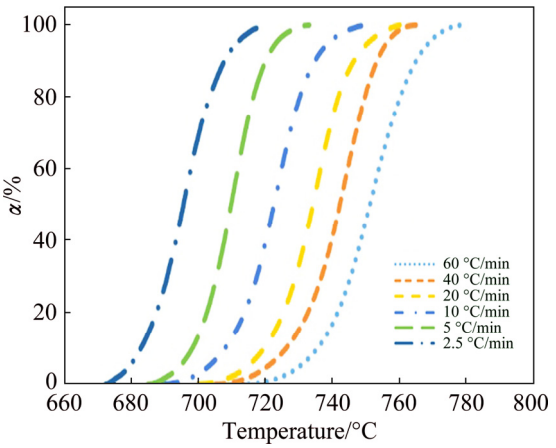

Fig. 3 Degree of crystallization, α, as function of temperature at different heating rates

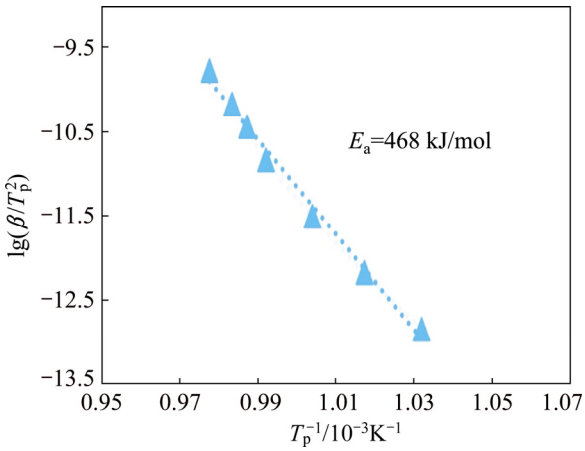

Fig. 4 Kissinger plot for crystallization of $Ni_{55}Nb_{35}Si_{10}$ amorphous powder

3.2.2 Evaluation of activation energy using iso-conversion models

In order to investigate the variation of the local activation energy, $E_a(\alpha)$, with degree of crystallization, the activation energies at different values of α are calculated using FWO and KAS iso-conversional methods. Accurate evaluation of activation energies is necessary to understand the crystallization process and

the mechanisms of nucleation and growth in amorphous alloys.

As shown in Fig. 5, the both methods show a gradual decrease in $E_a(\alpha)$ as the temperature increases. The KAS and FWO methods agree very well in the values of activation energies and their dependences with degree of crystallization.

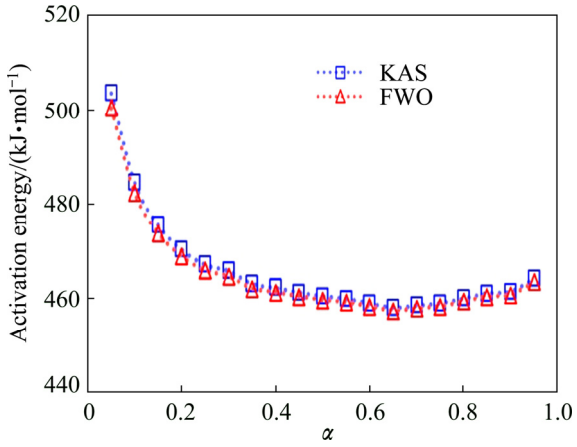

Fig. 5 Local activation energy for amorphous $Ni_{55}Nb_{35}Si_{10}$ alloy crystallization, as function of crystallized fraction

High values of activation energies at the beginning of crystallization indicate that a lot of atoms rearrange at the early stage of structural transformation. As atomic diffusion in Ni−Nb−Si system is difficult, especially at low temperature, the Ni−Nb−Si amorphous alloy exhibits high thermal stability. It was known that the presence of Si makes atomic diffusivity more difficult due to the atomic metal–metalloid pairing in Ni−Nb−Si system [13].

As shown in Fig. 5, the values of $E_a(\alpha)$ strongly decreased with crystallized fraction, α, in the range of $0.05<\alpha<0.35$ for both methods, indicating that crystallization rate increased as the temperature increased. Variation of the activation energy with temperature can be explained based on the theory proposed by TURNBULL and FISHER [22]. They determined the rate of crystallization in term of the nucleation rate and diffusivity, which both have different activation energies.

According to Eq. (3), the values of Avrami exponent, $n(\alpha)$, were determined from the slopes of linear plots $\ln[-\ln(1-\alpha)]$ versus $\ln\beta$ at different temperatures [23]:

$$\ln[-\ln(1-\alpha)]=\ln\chi(T)-n\ln\beta \quad (3)$$

where n is the Avrami exponent.

The following formula was obtained after the transformation of Eq. (3) at temperature T:

$$-\left.\frac{\mathrm{d}\{\ln[-\ln(1-\alpha)]\}}{\mathrm{d}\ln\beta}\right|_T=n \quad (4)$$

It can be seen that, in the range of $1<n<2.67$, the exponent decreases as the temperature increases. The Avrami exponent provides detailed information of the nucleation and growth mechanisms. RANGANATHAN and HEIMENDAHL [24] suggested that Avrami exponent could be expressed as: $n=a+bc$ where a is the nucleation index, which can be in the range of 0−1 ($a=0$ for a nucleation rate of zero, $0<a<1$ for a decreasing nucleation rate with time, $a=1$ for a constant nucleation rate and $a>1$ for an increasing nucleation rate), b is the dimension of the growth (with values 1, 2, or 3 for one-, two-, three-dimensional growth, respectively), and c is the growth index ($c=1$ for interface-controlled growth and $c=0.5$ for diffusion controlled growth).

According to Fig. 6, the Avrami exponents varied with temperature ranging from 2.67 to 1, which implies that the crystallization mechanism varies with temperature during non-isothermal annealing. It can be seen that the Avrami exponent during the main regime of crystallization (below 730 °C) lies between 1.5 and 2.5, indicating the decreasing nucleation rate for crystallization with time. Therefore, the governing mechanism of crystallization below 730 °C should be compatible with the decreasing nucleation rate with time. The Avrami exponent values decrease to 1 when the temperature increases to 746 °C. In the final stage of crystallization $n(\alpha)$ is lower than 1.5, indicating that the growth of nuclei and crystals dominated in the process [25].

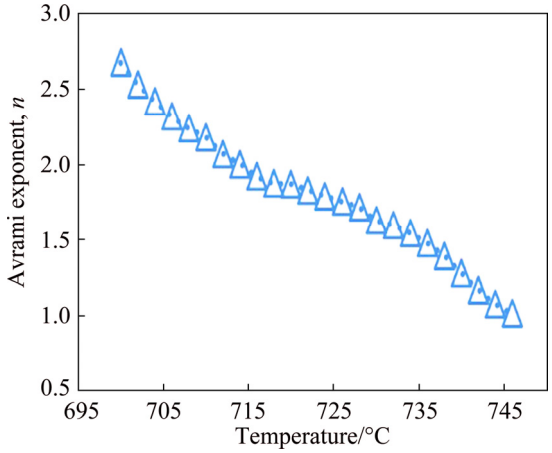

Fig. 6 Variation of Avrami exponent as function of temperature

According to Malek proposal [26], the applicability of the Johnson–Mehl–Avrami (JMA) model to describe the crystallization process can be tested by a simple criterion as follows. If the maximum of $z(\alpha)$ function falls into the range of 0.61−0.65, then JMA model is valid for non-isothermal kinetics study and if $\alpha_{max,z}$ shifted to a lower value then the condition of the validity is not fulfilled. In the present study, we have calculated both $z(\alpha)$ and $y(\alpha)$ functions as expressed in following equations [27]:

$$z(\alpha)=\frac{\mathrm{d}\alpha}{\mathrm{d}t}T\left[\frac{\pi(x)}{\beta}\right] \quad (5)$$

$$y(\alpha)=\frac{\mathrm{d}\alpha}{\mathrm{d}t}\exp x \quad (6)$$

where t represents time, $x=E_a/(RT)$, and $\pi(x)$ is a function of temperature integral and can be determined by Senum−Yang approximation [27]:

$$\pi(x)=\frac{x^3+18x^2+99x+96}{x^4+20x^3+120x^2+240x+120} \quad (7)$$

Figure 7 represents the variation of $y(\alpha)$ and $z(\alpha)$ with crystallized fraction, α, at different heating rates. As shown in Fig. 7 and Table 1, the maximum value of $z(\alpha)$ falls in the range of 0.53−0.57; whereas that of $y(\alpha)$ falls in the range of 0.38−0.42. The values of $\alpha_{\max,z}$ in the present study are smaller than the finger print of the JMA model predicted by Malek. Thus, according to Malek model, JMA model is not applicable to describe the crystallization kinetics of Ni−Nb−Si glass in the present case.

Therefore, the more generalized Sestak−Berggren SB(M,N) autocatalytic model was used to analyze the crystallization kinetics of Ni−Nb−Si alloy [28]:

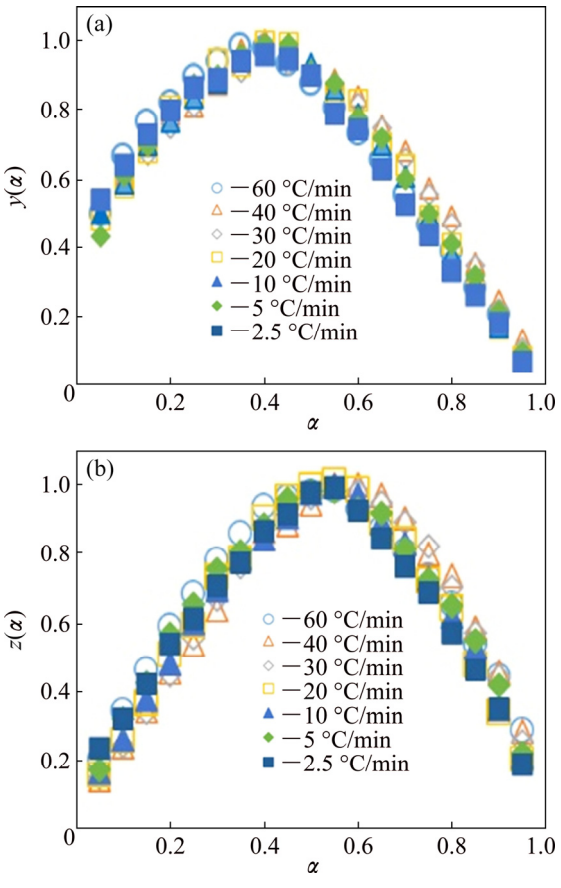

Fig. 7 Normalized $y(\alpha)$ (a) and $z(\alpha)$ (b) functions corresponding to non-isothermal measurements with crystallized fraction for different heating rates

Table 1 Values of maximum conversion fractions at different heating rates in $z(\alpha)$ and $y(\alpha)$ graphs

Heating rate/(°C·min^{-1})	$\alpha_{\max,z}$	$\alpha_{\max,y}$
2.5	0.54	0.38
5	0.54	0.39
10	0.55	0.39
20	0.55	0.40
30	0.56	0.42
40	0.57	0.42
60	0.53	0.38

$$f(\alpha)=\alpha^M(1-\alpha)^N \quad (8)$$

The kinetics exponent M and N are parameters that denote the relative contribution of acceleratory and deacceleratory part of the crystallization process. The parameters of this model can be expressed as a function of $\alpha_{\max,y}$ by [29]

$$\frac{M}{N}=\frac{\alpha_{\max,y}}{1-\alpha_{\max,y}} \quad (9)$$

The rate of the kinetic process is commonly expressed as a function of temperature (T) and extent of conversion (α) as follows [30]:

$$\frac{\mathrm{d}\alpha}{\mathrm{d}t}=A\exp\left(\frac{-E_a}{RT}\right)f(\alpha) \quad (10)$$

where A the pre-exponential factor, and $f(\alpha)$ a function that represents the reaction model.

Combining Eqs. (8) and (10) yields

$$\ln\left[\left(\frac{\mathrm{d}\alpha}{\mathrm{d}t}\right)\exp\left(\frac{E}{RT}\right)\right]=\ln A+N\ln[\alpha^{M/N}(1-\alpha)] \quad (11)$$

It should be noted that this model is physically meaningful only for M<1 [28]. Values of M, N and A were determined by analyzing DSC traces and fitting in Eq. (11) (Table 2). The average values of M, N and A are 0.626, 1.147 and 5.97×10^{24}, respectively. Therefore, the following kinetic equation for the reaction rate of nano-crystallization in amorphous Ni−Nb−Si alloy is suggested:

$$\frac{\mathrm{d}\alpha}{\mathrm{d}t}=5.97\times10^{24}\exp\left(\frac{-468000}{RT}\right)\alpha^{0.626}(1-\alpha)^{1.147} \quad (12)$$

The reaction rate as a function of temperature for different heating rates is plotted in Fig. 8. In order to check the validity of the prediction model, experimental results are also shown in Fig. 8 for comparison. A convincing consistency between the experimental results and simulated data, generated by SB model, are observed.

Table 2 Values of fitting parameters in autocatalytic model obtained by using mean value of activation energy (468 kJ/mol)

Heating rate/(°C·min^{-1})	M	N	ln(A/min^{-1})
2.5	0.505	1.172	57.031
5	0.625	1.123	57.089
10	0.684	1.231	57.001
20	0.719	1.255	57.094
30	0.703	1.131	57.086
40	0.630	1.000	57.050
60	0.518	1.121	56.981

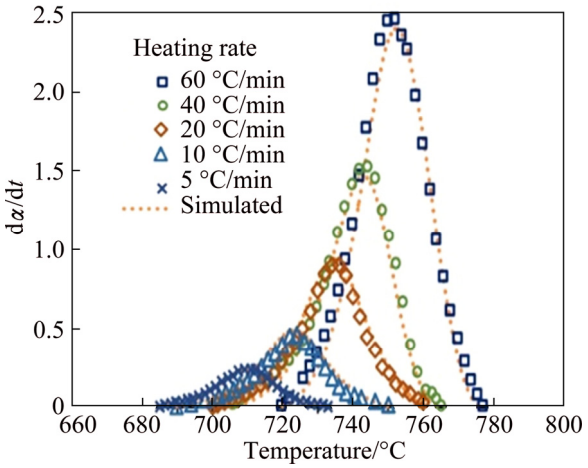

Fig. 8 Reaction rate as function of temperature for Ni−Nb−Si amorphous alloy

4 Conclusions

(1) Crystallization of the $Ni_{55}Nb_{35}Si_{10}$ amorphous alloy led to the formation of nano-crystals with dimension less than 10 nm in the amorphous matrix after annealing at 900 °C for 1 h.

(2) Formation of nano-crystals during crystallization is mainly governed by three-dimensional diffusion controlled growth of nuclei.

(3) The apparent activation energy of crystallization, evaluated through the Kissinger equation, was 468 kJ/mol. The large activation energy of crystallization of $Ni_{55}Nb_{35}Si_{10}$ amorphous alloy indicates its high thermal stability. Activation energy of crystallization process showed a decreasing trend during the first part of the process and remained almost constant during the second part.

(4) A model was developed to predict progression of the process quantitatively as follows:

$$\frac{\mathrm{d}\alpha}{\mathrm{d}t}=5.97\times10^{24}\exp\left(\frac{-468000}{RT}\right)\alpha^{0.626}(1-\alpha)^{1.147}$$

Acknowledgments

This research was supported by the Future Material Discovery Program of the National Research Foundation of Korea (NRF) funded by the Ministry of Science, ICT and Future Planning (MSIP) of Korea (2016M3D1A1023532)

References

[1] GUO S F, PAN F S, ZHANG H J, ZHANG D F, WANG J F, MIAO J, SU C, ZHANG C. Fe-based amorphous coating for corrosion protection of magnesium alloy [J]. Materials & Design, 2016, 108: 624−631.

[2] SHIRASAWA N, TAKIGAWA Y, UESUGI T, HIGASHI K. The evaluation parameters for glass-forming ability in Ti−Cu system metallic glasses [J]. Materials Letters, 2015, 139: 73−76.

[3] HAN Jia-jia, WANG Cui-ping, KOU Sheng-zhong, LIU Xing-jun. Thermal stability, crystallization behavior, Vickers hardness and magnetic properties of Fe−Co−Ni−Cr−Mo−C−B−Y bulk metallic glasses [J]. Transactions of Nonferrous Metals Society of China, 2013, 23: 148−155.

[4] ZHANG Jia-jia, LIU Wen-sheng, MA Yun-zhu, YE Xiao-shan, WU Ya-yu, HUANG Bo-yun. Preparation and properties of Ni68.6W17.9B13.5 metallic glass [J]. Transactions of Nonferrous Metals Society of China, 2015, 25: 1575−1579.

[5] DÉO L P, de OLIVEIRA M F. Accuracy of a selection criterion for glass forming ability in the Ni−Nb−Zr system [J]. Journal of Alloys and Compounds, 2014, 615: s23−s28.

[6] MA Y, YE J H, PENG G J, WEN D H, ZHANG T H. Nanoindentation study of size effect on shear transformation zone size in a Ni−Nb metallic glass [J]. Materials Science and Engineering A, 2015, 627: 153−160.

[7] LESZ S, DERCZ G. Study on crystallization phenomenon and thermal stability of binary Ni−Nb amorphous alloy [J]. Journal of Thermal Analysis and Calorimetry, 2016, 126: 19−26.

[8] SURYANARAYANA C. Mechanical alloying and milling [J]. Progress in Materials Science, 2001, 46: 1−184.

[9] KOCH C C, CAVIN O B, MCKAMEY C G, SCARBROUGH J O. Preparation of amorphous $Ni_{60}Nb_{40}$ by mechanical alloying [J]. Applied Physics Letters, 1983, 43: 1017−1019.

[10] CHEN Gang, FERRY M. Crystallization of Mg-based bulk metallic glass [J]. Transactions of Nonferrous Metals Society of China, 2006, 16: 833−837.

[11] ZHANG J, TENG X, XU S, GE X, LENG J. Temperature dependence of resistivity and crystallization behaviors of amorphous melt-spun ribbon of $Mg_{66}Zn_{30}Gd_4$ alloy [J]. Materials Letters, 2017, 189: 17−20.

[12] CZEPPE T. Mechanism and kinetics of nano-crystallization of the thermally stable NiNb(ZrTi)Al metallic glasses [J]. Journal of Thermal Analysis and Calorimetry, 2010, 101: 615−622.

[13] MINOUEI H, AKBARI G H, ENAYATI M H, HONG S I. Amorphization and nanocrystallization of Ni−Nb−Si alloys [J]. Materials Science and Engineering A, 2017, 682: 396−401.

[14] STARNIK M J. Analysis of aluminium based alloys by calorimetry: Quantitative analysis of reactions and reaction kinetics [J]. International Materials Reviews, 2004, 49: 191−226.

[15] BLAZQUEZ J S, CONDE C F, CONDE A. Non-isothermal approach to isokinetic crystallization processes: Application to the nanocrystallization of HITPERM alloys [J]. Acta Materialia, 2005, 53: 2305−2311.

[16] VYAZOVKIN S, BURNHAM A K, CRIADO J M, PÉREZ-MAQUEDA L A, POPESCU C, SBIRRAZZUOLI N.

ICTAC kinetics committee recommendations for performing kinetic computations on thermal analysis data [J]. Thermochimica Acta, 2011, 520: 1−19.
[17] KISSINGER H E. Reaction kinetics in differential thermal analysis [J]. Analytical Chemistry, 1957, 29: 1702−1706.
[18] AKAHIRA T, SUNOSE T. Method of determining activation deterioration constant of electrical insulating materials [J]. Research Report Chiba Institute of Technology, 1971, 16: 22−31.
[19] OZAWA T. A New method of analyzing thermogravimetric data [J]. Bulletin of the Chemical Society of Japan, 1965, 38: 1881−1886.
[20] FLYNN J H, WALL L A. Thermal analysis of polymer by thermogravimetric analysis [J]. Journal of Research of the National Bureau of Standards Section A, 1966, 70: 487−523.
[21] KIM S M, CHANDRA D, PAL N K, DOLAN M D, CHIEN W M, TALEKAR A, LAMB J, PAGLIERI S N, FLANAGAN T B. Hydrogen permeability and crystallization Kinetics in amorphous Ni−Nb−Zr alloys [J]. International Journal of Hydrogen Energy, 2012, 37: 3904−3913.
[22] TURNBULL D, FISHER J C. Rate of nucleation in condensed systems [J]. Journal of Chemical Physics, 1949, 17: 71−73.
[23] MATUSITA K, SAKKA S. Study on crystallization kinetics in glass by differential thermal analysis [J]. Thermochimica Acta, 1979, 33: 351−354.
[24] RANGANATHAN S, HEIMENDAHL M V. The three activation energies with isothermal transformations: applications to metallic glasses [J]. Journal of Materials Science, 1981, 16: 2401−2404.
[25] DOHERTY R D. Diffusive phase transformations in the solid state [C]//CAHN R W, HAASEN P. Physical metallurgy. Amsterdam, North-Holland: 1996: 1363−1506.
[26] SENUM G I, YANG R T. Rational approximations of the integral of the Arrhenius function [J]. Journal of Thermal Analysis and Calorimetry, 1977, 11: 445−447.
[27] MALEK J. The kinetic analysis of non-isothermal data [J]. Thermochimica Acta, 1992, 200: 257−269.
[28] MALEK J, CRIADO J M. The boundary conditions for kinetic models [J]. Thermochimica Acta, 1989, 153: 429−432.
[29] SVOBODA R, MALEK J. Interpretation of crystallization kinetics results provided by DSC [J]. Thermochim Acta, 2011, 526: 237−251.
[30] BROWN M E, DOLIMORE D, GALWEY A K. Reactions in the Solid State [M]. Vol. 22. Amsterdam: Elsevier, 1980.

非晶态 $Ni_{55}Nb_{35}Si_{10}$ 合金的非等温纳米结晶动力学

H. MINOUEI[1], G. H. AKBARI[1], M. H. ENAYATI[2], S. I. HONG[3]

1. Department of Metallurgy and Materials Science, Shahid Bahonar University, Kerman, Iran;
2. Department of Material Engineering, Nanotechnology and Advanced Material Institute, Isfahan University of Technology (IUT), Isfahan, Iran;
3. Department of Nanomaterials Engineering, Chungnam National University, Daejeon 305-764, Korea

摘　要：采用差示扫描量热法(DSC)研究机械合金化制备的 $Ni_{55}Nb_{35}Si_{10}$ 非晶合金的非等温结晶动力学。结果表明，该非晶合金在加热过程中表现出单级结晶，导致非晶态基体中形成金属间化合物纳米晶体。由基辛格方程确定的合金结晶表观活化能较高(468 kJ/mol)，说明该非晶合金具有较高的热稳定性。采用等转换法对结晶过程中活化能的变化进行研究，活化能从结晶开始一直缓慢降低至结晶分数 α=0.35，然后几乎保持不变直至结晶结束。通过测定 Avrami 指数，解释非晶合金非等温结晶的纳米结晶机理。透射电镜研究表明，在退火过程中通过纳米结晶可对非晶态合金进行微观结构调控。成核速率随时间的延长而减小，结晶机理主要受三维扩散控制生长支配。在 Sestak−Berggren 自催化模型的基础上，得到定量描述非等温结晶动力学的预测方程。

关键词：非晶合金；动力学；纳米结晶；DSC；活化能

(Edited by Bing YANG)